

A method for studying electron-density-based dynamics of many-electron systems in scaled cylindrical coordinates

Abhijit Poddar^{1,3} and B M Deb^{2,4}

¹ Indian Institute of Science Education & Research, HC-VII, Sector III, Salt Lake, Kolkata-700 106, India

² S N Bose National Centre for Basic Sciences, JD Block, Sector III, Salt Lake, Kolkata-700 098, India

E-mail: bmdeb@yahoo.co.in

Received 31 October 2006, in final form 5 April 2007

Published 14 May 2007

Online at stacks.iop.org/JPhysA/40/5981

Abstract

The combination of quantum fluid dynamics and density functional theory had led to the formulation of a single time-dependent equation, the generalized nonlinear Schrödinger equation (GNLSE). In this paper, the above GNLSE is written as a nonlinear diffusion-type equation in appropriately scaled cylindrical coordinates and evolved in imaginary time to obtain the electronic energies, densities and other properties of all the noble gas atoms. The close agreement of the values obtained with those from the literature implies that the same method can be used in real time to study the density-based dynamics of many-electron systems in axially symmetric external fields such as intense laser fields, with relatively less computational effort.

PACS numbers: 31.15.Ew, 31.70.Hq, 32.10.-f, 31.15.Fx, 31.15.-p

1. Introduction

In recent years, there have been efforts to calculate the static as well as dynamic (time-dependent) electron densities of many-electron systems *through a single equation* within the framework of density functional theory (DFT) [1–3]. The earliest attempt is the Thomas–Fermi method [4, 5] in which static electron densities are calculated by making use of a single equation. A dynamical single equation formulation was achieved by combining [6] quantum fluid dynamics (QFD) and DFT. It was shown that the two basic QFD equations, namely,

³ On leave from Surendranath Evening College, Kolkata-700 009, India.

⁴ Also from the Jawaharlal Nehru Centre for Advanced Scientific Research, Bangalore-560 064, India. Address from May 2007: Indian Institute of Science Education & Research, HC-VII, Sector III, Salt Lake, Kolkata-700 106, India.

the equation of continuity and an Euler-type equation of motion, can be merged to yield a single time-dependent generalized nonlinear Schrödinger equation (GNLSE). There have been other time-dependent formulations such as the self-interaction-free time-dependent DFT [7, 8] and time-dependent current DFT [9] which, however, deal with individual occupied spin orbitals that render themselves computationally highly demanding, especially when dealing with systems with a relatively large number of electrons. The QFD–DFT approach had been subsequently used to obtain the ground-state densities in spherical coordinates [10–12] as well as to study dynamical properties of two-electron systems [13–16]. There has also been an abiding interest in studying the static and dynamic properties of noble gas atoms and clusters, especially the phenomenon of above-threshold ionization (ATI), high-order harmonic generation (HHG), unusual stabilization, etc, in intense laser fields [17–21]. The QFD–DFT approach has been tested on such systems to study their ground-state properties by Roy and Chu [12] using a time-dependent generalized pseudospectral technique. They have also applied this technique to study multiphoton ionization (MPI) and HHG of He and Ne atoms in intense laser fields [17]. While such calculations in one dimension have yielded considerable insights into ultrafast processes, they might obscure some of the actual physics of these phenomena, particularly in the attosecond domain [21]. There is clearly a need to choose a more realistic and flexible coordinate system.

In this paper, the GNLSE is recast as a nonlinear diffusion equation in *scaled cylindrical coordinates* (compared to previous works employing ordinary cylindrical coordinates [13–16]) and evolved in imaginary time to obtain the ground-state electron densities, energies and other properties of all the noble gas atoms. The results are compared with literature values for testing the potential efficacy of the present formulation in studying ultrafast dynamical processes involving atoms and molecules, with a relatively large number of electrons, in real time and three dimensions. Since the scaling can be suitably adjusted depending on the problem/system, this is a more flexible approach.

2. Methodology

The QFD equations involving the two dynamical variables in three-dimensional space, namely, the electron density $\rho(\mathbf{r}, t)$ and the current density $\mathbf{j}(\mathbf{r}, t)$, are expressed as (atomic units have been used throughout)

$$\frac{\partial \rho(\mathbf{r}, t)}{\partial t} + \nabla \cdot \mathbf{j}(\mathbf{r}, t) = 0 \quad (1)$$

$$\frac{\partial \chi(\mathbf{r}, t)}{\partial t} + \frac{1}{2}(\nabla \chi)^2 + \frac{\delta G[\rho]}{\delta \rho} + \int \frac{\rho(\mathbf{r}', t)}{|\mathbf{r} - \mathbf{r}'|} d\mathbf{r}' + v(\mathbf{r}, t) = 0, \quad (2)$$

where $\mathbf{j}(\mathbf{r}, t) = \rho \nabla \chi(\mathbf{r}, t)$, with χ being the velocity potential (see later). The term $v(\mathbf{r}, t)$ consists of the electron–nuclear attraction potential and the potential due to any external field. The fourth term is the classical inter-electronic Coulomb repulsion potential $v_{\text{el}--\text{el}}$. The universal functional $G[\rho]$, comprising kinetic, exchange and correlation energy functionals, can be written as

$$G[\rho] = \frac{1}{8} \int \frac{|\nabla \rho|^2}{\rho} d\mathbf{r} + T_{\text{correc}}[\rho] + E_x[\rho] + E_c[\rho]. \quad (3)$$

The first term on the right-hand side of equation (3) is the Weizsäcker kinetic energy functional while the second term is a correction to the first term to properly account for not only the total kinetic energy of an N -electron ($N > 2$) system but also its global and local behaviour,

including the atomic shell structure [22]. The remaining two terms are the exchange and correlation energy functionals, respectively.

By defining a complex hydrodynamical ‘wavefunction’ as

$$\psi(\mathbf{r}, t) = \rho^{1/2}(\mathbf{r}, t) \exp[i\chi(\mathbf{r}, t)], \quad (4)$$

equations (1) and (2) can be combined to arrive at a *single* time-dependent generalized nonlinear Schrödinger equation (GNLSE) [6] for many-electron systems,

$$\left[-\frac{1}{2}\nabla^2 + v_{\text{eff}}(\rho; \mathbf{r}, t) \right] \psi(\mathbf{r}, t) = i \frac{\partial \psi(\mathbf{r}, t)}{\partial t}, \quad i = \sqrt{-1}, \quad (5)$$

where $v_{\text{eff}}(\rho; \mathbf{r}, t)$ is the sum of all the potential terms given below. The function $\chi(\mathbf{r}, t)$ in equation (4) has been called the velocity potential⁵ in quantum fluid dynamics literature. Equation (5) may appear to have the same form as the Gross–Pitaevskii equation (GPE) [23, 24] for Bose–Einstein condensate. However, it may be noted that while the GPE is a cubic (in ψ) Schrödinger equation, equation (5) is more complicated, having both integer and noninteger powers of ψ as well as nonlinear integral operators occurring due to the kinetic, Coulomb, exchange and correlation terms in v_{eff} . It may be further noted that, irrespective of the number of electrons in the many-electron system, equation (5) requires one to solve only a single one-particle equation (with two-particle effects embedded in it) for the entire system. Thus, equation (5) defines a single ‘orbital’ for the whole system, yielding a total one-electron density.

Assuming the validity of equation (5) in imaginary time τ , the former is first written in τ ; then τ is replaced by $-it$ where t is real time. This transforms equation (5) into a nonlinear diffusion-type equation

$$\left[-\frac{1}{2}\nabla^2 + v_{\text{eff}}(\rho; \mathbf{r}, t) \right] R(\mathbf{r}, t) = -\frac{\partial R(\mathbf{r}, t)}{\partial t} \quad (6)$$

in real time. In equation (6), $R(\mathbf{r}, t)$ is a real diffusion function different from the complex function $\psi(\mathbf{r}, t)$. By numerically solving equation (6) for a sufficiently long time and forcing normalization after every iteration, one eventually reaches the stationary ground state of the system corresponding to a globally minimum energy value. This is the well-known diffusion-quantum Monte Carlo (DQMC) approach (see, e.g., [11, 16, 25–29]).

The effective potential $v_{\text{eff}}(\rho; \mathbf{r}, t)$ in equation (5) is the sum of the following potential terms:

$$v_{\text{eff}}(\rho; \mathbf{r}, t) = v_{\text{el-el}} + v_{\text{nu-el}} + v_x + v_c + v_{T_{\text{correc}}} + v_{\text{ext}}. \quad (7)$$

In equation (7), $v_{\text{el-el}} = \frac{\delta E_{\text{el-el}}}{\delta \rho}$ is the interelectronic Coulomb repulsion potential, with $E_{\text{el-el}}$ being the corresponding energy; $v_{\text{nu-el}} = \frac{\delta E_{\text{nu-el}}}{\delta \rho}$ is the nuclear–electron attraction potential, with $E_{\text{nu-el}}$ being the corresponding energy; $v_x = \frac{\delta E_x}{\delta \rho}$ and $v_c = \frac{\delta E_c}{\delta \rho}$ are the electron–electron exchange and correlation potentials, respectively, with E_x and E_c being the corresponding energies; $v_{T_{\text{correc}}} = \frac{\delta E_{T_{\text{correc}}}}{\delta \rho}$ is the potential corresponding to the kinetic energy correction term T_{correc} ; v_{ext} is the potential corresponding to the externally applied field.

The functional forms of the different components are as follows:

$$E_{\text{el-el}} = \frac{1}{2} \iint \frac{\rho(\mathbf{r}, t)\rho(\mathbf{r}', t)}{|\mathbf{r} - \mathbf{r}'|} d\mathbf{r} d\mathbf{r}', \quad (8)$$

⁵ The dimensions of a velocity potential are (velocity) (distance). If one does not employ atomic units, then the phase part of the hydrodynamical ‘wavefunction’ is $\exp[i\chi(\mathbf{r}, t)/\hbar]$ (see [3]). Therefore, for a particle of unit mass (electron in atomic units), $\chi(\mathbf{r}, t)$ has the dimensions of (velocity) (distance), with $\text{grad } \chi(\mathbf{r}, t)$ giving the velocity field.

$$v_{\text{el-el}}(\mathbf{r}, t) = \int \frac{\rho(\mathbf{r}', t)}{|\mathbf{r} - \mathbf{r}'|} d\mathbf{r}', \quad (9)$$

$$E_{\text{nu-el}} = - \int \frac{Z}{\mathbf{r}} \rho(\mathbf{r}, t) d\mathbf{r}, \quad (10)$$

$$v_{\text{nu-el}}(\mathbf{r}, t) = - \frac{Z}{\mathbf{r}}, \quad (11)$$

with Z being the nuclear charge of an atom. For He, the exact forms of the exchange energy and potential have been employed, namely,

$$E_{x_{\text{He}}} = - \frac{1}{4} \iint \frac{\rho(\mathbf{r}, t) \rho(\mathbf{r}', t)}{|\mathbf{r} - \mathbf{r}'|} d\mathbf{r} d\mathbf{r}', \quad (12)$$

$$v_{x_{\text{He}}}(\mathbf{r}, t) = - \frac{1}{2} \int \frac{\rho(\mathbf{r}', t)}{|\mathbf{r} - \mathbf{r}'|} d\mathbf{r}'. \quad (13)$$

For the other four noble gas atoms, a parameterized local exchange energy functional [10, 12, 30] has been used. A local parameterized Wigner-type functional [10, 12, 31] is used for the correlation energy of all the atoms. The kinetic energy correction and the corresponding potential are taken as modified Thomas–Fermi terms [10, 12, 22]. It may be noted that the evaluation of the interelectronic Coulomb repulsion potential in cylindrical coordinates poses a problem, especially for atoms with higher Z values. The Green's function $\frac{1}{|\mathbf{r} - \mathbf{r}'|}$ in equation (9) has been expressed in terms of the half-integer degree Legendre function of the second kind ($Q_{m-\frac{1}{2}}$) [32]:

$$\frac{1}{|\mathbf{r} - \mathbf{r}'|} = (1/(\pi \sqrt{\tilde{\rho} \tilde{\rho}'})) \sum_{m=-\infty}^{\infty} e^{im(\phi - \phi')} Q_{m-\frac{1}{2}}(\kappa), \quad (14)$$

where

$$\kappa = (\tilde{\rho}^2 + \tilde{\rho}'^2 + (z - z')^2) / (2\tilde{\rho}\tilde{\rho}') \quad (15)$$

and $\tilde{\rho}'$ as well as z' correspond to \mathbf{r}' . Equation (14) can be equivalently expressed as

$$\frac{1}{|\mathbf{r} - \mathbf{r}'|} = (1/(\pi \sqrt{\tilde{\rho} \tilde{\rho}'})) \sum_{m=0}^{\infty} \epsilon_m \cos[m(\phi - \phi')] Q_{m-\frac{1}{2}}(\kappa), \quad (16)$$

where ϵ_m is the Neumann factor [33]. Substituting equation (16) into equation (9) and noting that $m = 0$ for an axially symmetric system, one obtains

$$v_{\text{el-el}}(\mathbf{r}, t) = (1/(\pi \sqrt{\tilde{\rho}})) \int \frac{\rho(\mathbf{r}')}{\sqrt{\tilde{\rho}'}} Q_{-\frac{1}{2}}(\kappa) d\mathbf{r}', \quad (17)$$

where $Q_{-\frac{1}{2}}(\kappa)$ is expressed in terms of the complete elliptic integral of the first kind $K(\mu)$ [34], namely

$$Q_{-\frac{1}{2}}(\kappa) = \mu K(\mu), \quad (18)$$

where

$$\mu = \sqrt{2/(1 + \kappa)}. \quad (19)$$

The above procedure is employed to calculate the classical Coulomb potential $v_{\text{el-el}}$ at the grid boundaries. For the interior points of the cylindrical mesh, the values of $v_{\text{el-el}}$ are obtained from the solution of the Poisson equation

$$\nabla^2 v_{\text{el-el}} = -4\pi\rho \quad (20)$$

with the values at the boundaries serving as Dirichlet boundary conditions.

3. Numerical solution of the diffusion equation in scaled cylindrical coordinates

In order to solve equation (6) in ordinary cylindrical coordinates $\bar{\rho}$ and z , scaled cylindrical coordinates [35, 36] ξ and ζ are employed, where

$$\bar{\rho} = \xi^\lambda \quad (21)$$

and

$$z = g(\zeta) = [1 - (1 - \beta) \exp(-\zeta^2/\gamma^2)]\zeta, \quad (22)$$

where λ , β and γ are the adjustable parameters. It may be noted that the equal spacings in the scaled coordinates ensure a greater number of $\bar{\rho}$ and z points near the origin. This helps in tackling steep Coulomb potentials near the origin, especially for atoms with high Z . The diffusion function R must satisfy the normalization condition

$$2\pi \int |R|^2 \bar{\rho} d\bar{\rho} dz = N, \quad (23)$$

where N is the total number of electrons and the factor 2π results from integration over the azimuthal angle. In order that the above normalization condition is satisfied in the scaled coordinate system, a transformed diffusion function R' is employed, where

$$R' = \sqrt{\lambda} \xi^{\lambda - \frac{1}{2}} R. \quad (24)$$

Note that the transformed function R' is zero at the origin thereby ensuring that numerical difficulties are not encountered at this Coulomb singularity.

In scaled cylindrical coordinates and in terms of the scaled function $R'(\mathbf{r}, t)$, equation (6) can be written as

$$\hat{L}R'(\mathbf{r}, t) = -\frac{\partial R'(\mathbf{r}, t)}{\partial t}, \quad (25)$$

where $\hat{L} = -\frac{\partial}{\partial t}$ contains all the differential operators in the scaled coordinates and the effective potential term. The Taylor expansion of $R'(\mathbf{r}, t + \Delta t)$ about $R'(\mathbf{r}, t)$ can then be expressed as

$$R'(\mathbf{r}, t + \Delta t) = \exp\left(\Delta t \frac{\partial}{\partial t}\right) R'(\mathbf{r}, t) = \exp(-\Delta t \hat{L}) R'(\mathbf{r}, t). \quad (26)$$

The evolution operator $\exp(-\Delta t \hat{L}) R'(\mathbf{r}, t)$ is real and non-unitary. \hat{L} is split along the lines of Peaceman and Rachford [6, 37] as follows:

$$\hat{L} = \hat{A} + \hat{B}, \quad (27)$$

where

$$\hat{A} = K_\zeta + \frac{1}{2} v_{\text{eff}} \quad (28)$$

and

$$\hat{B} = K_\xi + \frac{1}{2} v_{\text{eff}} \quad (29)$$

with

$$\hat{K}_\xi = -\frac{1}{2} \left[\lambda^{-2} \xi^{2-2\lambda} \frac{\partial^2}{\partial \xi^2} - 2\lambda^{-2} \xi^{1-2\lambda} (\lambda - 1) \frac{\partial}{\partial \xi} + \lambda^{-2} \xi^{-2\lambda} \left(\lambda - \frac{1}{2} \right)^2 \right] \quad (30)$$

and

$$\hat{K}_\zeta = -\frac{1}{2} \left[g'^{-2} \frac{\partial^2}{\partial \zeta^2} - g'^{-3} g'' \frac{\partial}{\partial \zeta} \right]. \quad (31)$$

Writing $R'(\mathbf{r}, t + \Delta t)$ as R^{m+1} and $R'(\mathbf{r}, t)$ as R^m one obtains a symmetric form of equation (26) in terms of \hat{A} and \hat{B} , namely,

$$[1 + (\Delta t/2)\hat{A}][1 + (\Delta t/2)\hat{B}]R^{m+1} = [1 - (\Delta t/2)\hat{B}][1 - (\Delta t/2)\hat{A}]R^m. \quad (32)$$

Now, using Peaceman–Rachford alternate direction implicit (ADI) scheme (see [6] for an early application of this method) one can recast the above equation into two equations involving the value of R' at the fictitious intermediate time step $\frac{\Delta t}{2}$ as follows:

$$\left(1 + \frac{\Delta t}{2}\hat{B}\right)R^{m+\frac{1}{2}} = \left(1 - \frac{\Delta t}{2}\hat{A}\right)R^m \quad (33)$$

and

$$\left(1 + \frac{\Delta t}{2}\hat{A}\right)R^{m+1} = \left(1 - \frac{\Delta t}{2}\hat{B}\right)R^{m+\frac{1}{2}}. \quad (34)$$

The first- and second-order partial derivatives in equations (33) and (34) are approximated with two-point and three-point central difference formulae, respectively, leading to each of the above two equations being converted into a set of tridiagonal matrix equations which are then solved with the knowledge of the boundary conditions [38] to yield R^{m+1} from R^m . After each iteration, normalization is forced on R^{m+1} and a fresh iteration is started.

The values of the parameters in the scaled coordinates have been taken as follows: $\lambda = 1.5$, $\beta = 0.02$ and $\gamma = 14$. For Kr, however, the value of β has been taken as 0.01. The number of points N_1 and N_2 in the ξ and ζ directions, respectively, have been chosen as 601 and 601 for He, 801 and 801 for Ne, 1001 and 1001 for Ar and Xe. For Kr, 1051 points are used in both the directions. The ξ grid boundaries are taken as 1.0×10^{-6} and 0.6 and the ζ grid boundaries were taken as -16.0 and $+16.0$ for all the atoms. The temporal spacing Δt has been chosen as 0.000 05 for He and Ne; 0.000 01 for Ar and Xe. For Kr, $\Delta t = 0.75 \times 10^{-5}$. Note that the choice of a larger number of points and finer grids, generally for atoms with larger Z , yields better accuracy but at the cost of computation speed.

There are various ways of solving the Poisson equation (20) subject to Dirichlet boundary conditions. The present work employs a fast and efficient program named SEPELI, which is included in the FISHPACK [39] package of partial differential equation solvers freely available at the 'www.netlib.org' repository. The numerical solution has been launched by taking Slater-type functions [10] as input; these ensure a faster rate of convergence compared to other trial functions.

It may be noted that the present work reports the first numerical solution of equation (6) in scaled cylindrical coordinates, where the same set of parameters as reported in [10] have been employed for all the noble gas atoms, in contrast to a previous work on H^- , He, Ne and Ar, where different parameters were employed for different systems in ordinary cylindrical coordinates [40]⁶.

4. Results and discussion

The most satisfactory feature of the present approach is that all the calculated quantities maintain strict spherical symmetry, not only in their converged values at very long times, but also throughout the entire evolution process, in spite of the fact that the evolution is carried out in cylindrical and not spherical coordinates (figures 1–3).

⁶ The following values of the parameters concerned were employed in chapter 5 of the thesis instead of those reported in [10]: H^- , $b = 23.437$, $\alpha_X = 0.006\ 14$; He, $a = 10.81$, $\alpha_X = 0.0128$; Ne, $a = 9.82$, $\alpha_X = 0.0167$, $\alpha_1 = 77.475$, $\alpha_2 = 1.3152$; Ar, $a = 5.863$, $\alpha_X = 0.113\ 43$, $\alpha_1 = 73.8242$. The same work was reported in the second part of [40].

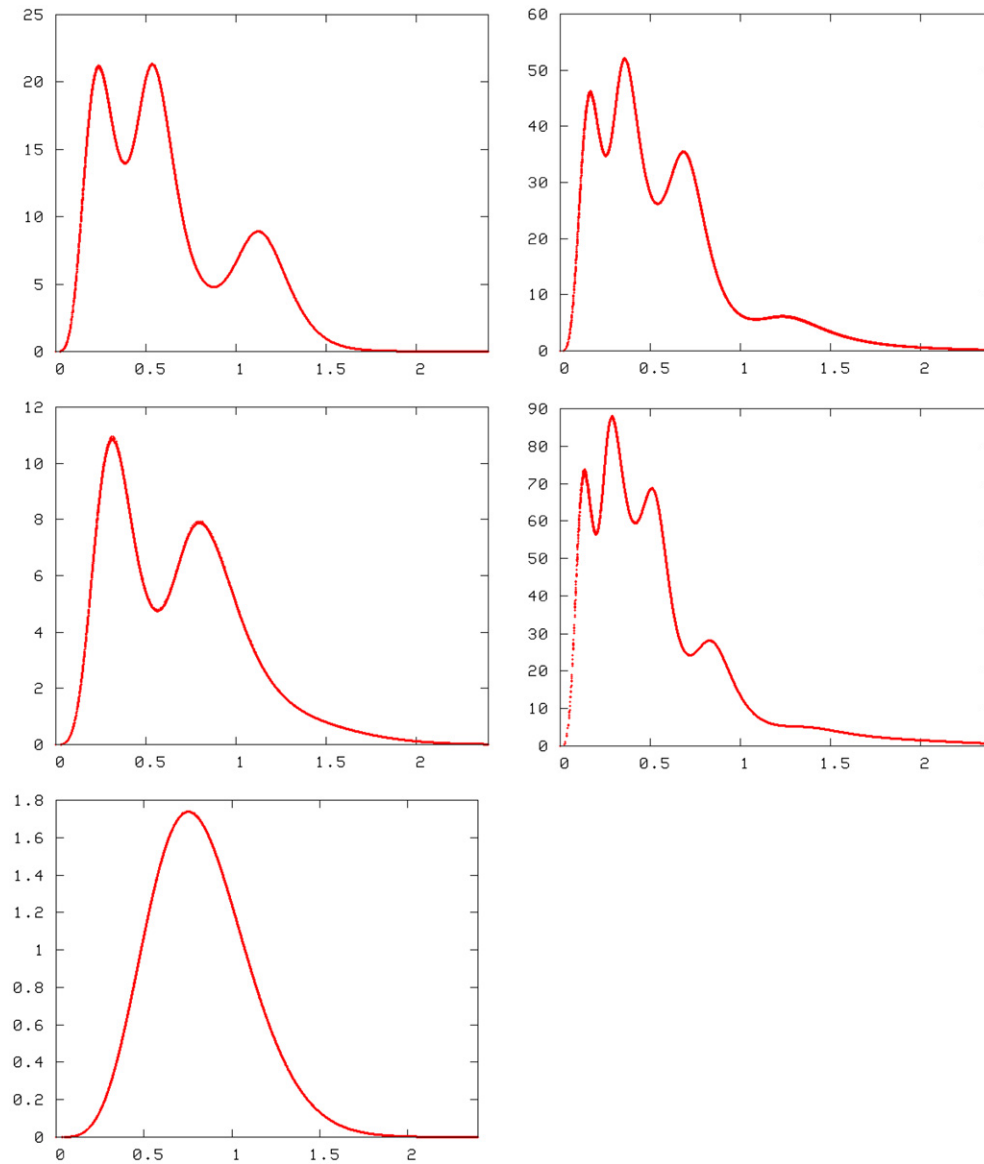


Figure 1. Plot of radial density (au) $4\pi r^2 \rho$ versus \sqrt{r} , where $r = \sqrt{\bar{\rho}^2 + \bar{z}^2}$ for each $\xi - \zeta$ point of the scaled cylindrical coordinate mesh (clockwise from bottom left) for He, Ne, Ar, Kr and Xe atoms, respectively, at convergence.

Figure 1 shows the spatial profile of the radial densities of He, Ne, Ar, Kr and Xe as a function of $r^{1/2}$, where r is the radial distance, calculated at all the $\xi - \zeta$ points of the scaled cylindrical grid after a sufficient number of iterations. The radial densities closely resemble those from Hartree–Fock (HF), Deb and Ghosh [19] as well as Roy and Chu [12], exhibiting their inherent shell structures, as expected. Figure 1 also shows how one may obtain strictly spherical densities after evolving the GNLSE for a sufficiently long time, in spite of our calculations resorting to finite differencing in scaled cylindrical coordinates. In order to obtain

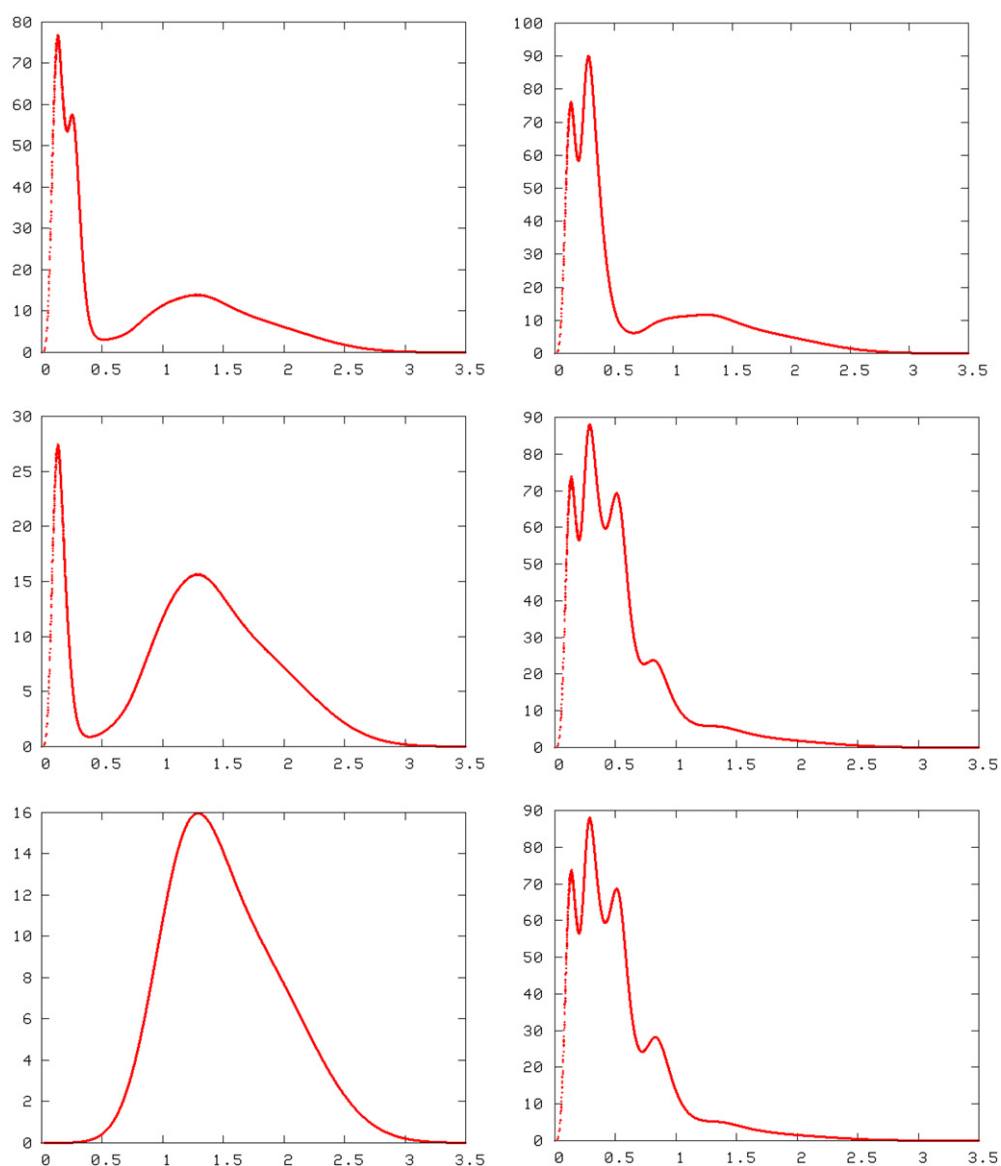


Figure 2. Plot of radial density (au) $4\pi r^2\rho$ versus \sqrt{r} for Xe atom, where $r = \sqrt{\tilde{\rho}^2 + z^2}$ for each $\xi - \zeta$ point of the scaled cylindrical coordinate mesh (clockwise from bottom left) at the start, after 300 time steps, after 600 time steps, after 1100 time steps, after 7000 time steps and at convergence, respectively.

a better insight into this aspect, figure 2 depicts the radial density plots for Xe at intermediate steps of the numerical evolution. One can observe how the spherical symmetry of the electron density is maintained throughout the evolution process and how the shell structure gradually makes its appearance. This maintenance of spherical symmetry validates the algorithm, the choice of the grid parameters λ , β , γ , the grid boundaries as well as the spatial and temporal grid spacings, $\Delta\xi$, $\Delta\zeta$ and Δt , respectively. It has also been observed that the algorithm is

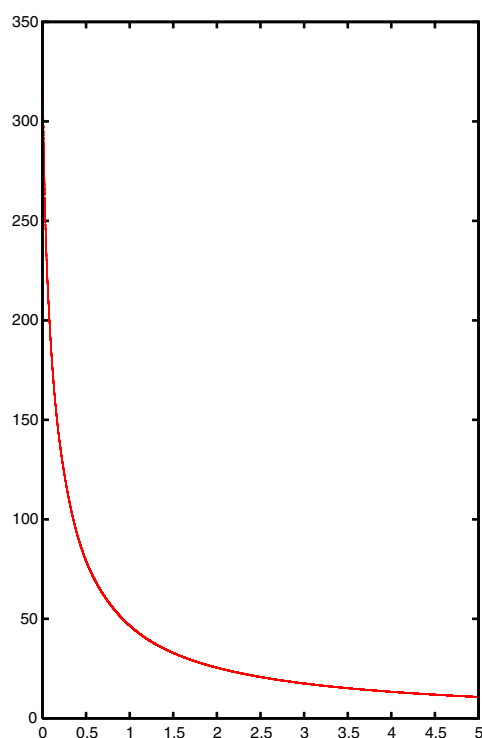


Figure 3. Plot of electron–electron repulsion potential (au) $v_{\text{el-el}}$ versus r for Xe atom, where $r = \sqrt{\rho^2 + z^2}$ for each $\xi - \zeta$ point of the scaled cylindrical coordinate mesh, at convergence. $v_{\text{el-el}}$ has been obtained from the solution of the Poisson equation for the interior mesh points of the grid using the ‘FISHPACK’ partial differential equation solver [39]. The values at the boundaries required for the solution are obtained through equation (17).

rather sensitive to the correlation of $\Delta\xi$ and $\Delta\zeta$ with Δt . Although, no analytical criterion for stability has been derived yet [27], we have found from extensive experimentation that $\Delta t \leq \Delta\xi \times \Delta\zeta$ yields quite accurate results.

The variations of different potential terms constituting v_{eff} , namely, $v_{\text{nu-el}}$, $v_{\text{el-el}}$, v_x , v_c and $v_{T_{\text{correc}}}$, with the radial distance are also studied. The nuclear–electron attraction potential $v_{\text{nu-el}}$ rapidly decreases as one approaches the Coulomb singularity at the origin. The use of appropriately scaled coordinates does ensure that this potential term is properly calculated at points close to the origin. The same holds true for the electron–electron repulsion potential $v_{\text{el-el}}$ as well as the exchange and correlation potentials v_x and v_c , respectively. It is gratifying to note that the plot of $v_{\text{el-el}}$ against r for Xe (figure 3) shows spherical symmetry, like those for the radial electron density, in spite of being calculated by using finite differences along scaled cylindrical coordinates. Expectedly, the other potential terms show spherical symmetry since they are calculated as functions of r , and hence their plots are not presented. Finally, $v_{T_{\text{correc}}}$ reveals a marked shell structure in its variation with r [22]. It may be recalled that this potential term is responsible for the shell structure in the radial density and therefore a proper choice of the potential arising from the kinetic energy correction term ($v_{T_{\text{correc}}}$) is essential for obtaining the correct electron density [22].

Table 1 presents the nonrelativistic ground-state energies and different energy components as obtained after evolving the diffusion equation, equation (6), for a sufficiently large number of iterations in scaled cylindrical coordinates. In all cases, the total energies go below the

Table 1. Ground-state properties (au) of noble gas atoms. PW denotes the present work while HF denotes the values obtained [10] by using Hartree–Fock density. The ‘exact’ nonrelativistic atomic energies (au), quoted in [10], are: He, 2.9037; Ne, 128.939; Ar, 527.540; Kr, 2753.8896; Xe, 7235.0512.

Property	Reference	He	Ne	Ar	Kr	Xe
$-E$	PW	2.9033	128.7422	527.3777	2753.0370	7234.8235
	HF	2.8617	128.5470	526.8174	2752.0546	7232.1302
	[10]	2.8973	128.9065	527.5486	2753.8809	7234.9742
$-E_{\text{nu-el}}$	PW	6.7676	307.6406	1267.6575	6519.2882	17199.8669
	HF	6.7492	311.1333	1255.0504	6582.5412	17164.9821
	[10]	6.7850	311.0597	1245.5699	6533.8352	17038.2385
$E_{\text{el-el}}$	PW	2.0565	61.7228	233.7806	1043.3978	2616.4803
	HF	2.0516	66.1476	231.6093	1172.3372	2880.0352
	[10]	2.0651	65.7129	220.6552	1119.3762	2744.7642
$-E_x$	PW	1.0282	11.7012	30.4347	89.4006	172.1502
	[10]	1.0325	12.1111	29.4850	91.5847	173.9435
$-E_c$	PW	0.0421	0.3391	0.7366	1.6760	2.7123
	[10]	0.0423	0.3561	0.7011	1.7529	2.8407
T_w	PW	–	95.1316	328.8362	1427.7328	3445.8170
	HF	–	90.6140	308.4206	1276.7349	2932.0548
	[10]	–	94.2068	322.0345	1377.5940	3226.9174
T_{correc}	PW	–	34.0841	208.8344	1386.1972	4077.6085
	HF	–	37.3886	214.4033	1465.2484	4298.9068
	Ref [10]	–	34.7006	205.5177	1376.3217	4008.3670
Virial, $-\langle V \rangle / \langle T \rangle$	PW	2.008	1.996	1.981	1.978	1.962
	HF	2.000	2.000	2.000	2.000	2.000
	[10]	2.000	2.000	2.000	2.000	2.000

corresponding Hartree–Fock values and are close to the ‘exact’ nonrelativistic as well as the one-dimensional results [10, 12]. Similar satisfactory agreements with literature values are observed for all the other calculated properties in table 1. For all these static results, the accuracy can be further improved by choosing finer spatial and temporal mesh sizes using larger computation times. However, note that the principal objective in developing the present method has been to eventually apply it for studying femto- and attosecond phenomena exhibited by atoms and molecules, with a relatively large number of electrons, under intense laser fields, where one would encounter cylindrical symmetry. Since this would involve the employment of coarser spatial and temporal mesh sizes as well as larger computation grids than those employed in this paper, our aim has been to test the present method for spherically symmetric systems and to see if the present results agree well with those obtained through the single-coordinate-based algorithms [10, 12]. As is evident from figures 1–3 and table 1, this has been achieved. Since the Weizsäcker kinetic energy is higher in Ne, Ar, Kr and Xe, the corresponding values of the virial constant ($-\langle V \rangle / \langle T \rangle$) becomes less than the ideal value of 2.0; higher values of T_{correc} also play a role here. This situation is a consequence of the finite-difference approximation, which can be improved by taking finer mesh sizes.

Finally, questions arise: (a) Why are the results in table 1 so satisfactory? (b) How can the calculations be extended to any many-electron system, namely, atoms, molecules,

clusters and solids? The answer to (a) lies primarily in the goodness of the various density functionals employed. By ‘goodness’ one implies numerical accuracy as well as satisfactory short-range and long-range behaviour of the density functionals. For example, the kinetic energy functional is taken as a sum of the Weizsäcker term and a modified Thomas–Fermi term, the latter giving $T_{\text{correc}}[\rho]$. For noble gas atoms, $T_{\text{correc}}[\rho]$ is simply modelled [10, 22], such that information about the shell structure is incorporated (note that a satisfactory universal functional for $T_{\text{correc}}[\rho]$ is still not available). The *local* exchange functional employed for the atoms with more than two electrons gives near-Hartree–Fock accuracy comparable to Becke’s gradient-corrected functional [30]. The *local* Wigner correlation functional also gives very good correlation energies for atoms and molecules (see, e.g., [10]). More importantly, since time dependence and excited states are intimately linked, the Wigner correlation functional has been remarkably successful in hybrid wavefunction–DFT calculations of numerous atomic excited states, involving very small to large excitation energies and including *autoionizing states* for which taking due account of electron correlation is crucial (for a review of such works on excited states, see [41]). It is, however, clear that the correction term to the kinetic energy $T_{\text{correc}}[\rho]$, which is about one-fourth to half the total kinetic energy in the present case and which dominates over the Weizsäcker term for Xe atom, is of utmost importance in obtaining the correct density.

Question (b) above emphasizes the *pressing need to find a satisfactory, universal form* for $T_{\text{correc}}[\rho]$. The present single-equation approach to calculate the static and dynamic electron densities would then be quite useful in studying structural and dynamical phenomena of many-electron systems. Unfortunately, this has remained an unsolved problem (see [42] for an early review on the kinetic energy problem). Therefore, although equation (5) is, in principle, applicable to any many-electron system, at present one needs to model $T_{\text{correc}}[\rho]$ for a particular class of systems, as has been done in this work (see also [10, 22]). Hopefully, new kinetic energy density functionals might emerge out of several recent, alternative lines of thought. For example, March [43] had earlier proposed a formally exact expression for the Pauli potential, involving both the electron density and its gradient, in terms of the Thomas–Fermi kinetic energy term, the Weizsäcker term and a term involving the Laplacian of the electron density. The behaviour of gradient approximations to the kinetic energy functional was studied by Handy *et al* [44, 45]. More general forms of the kinetic energy as a functional of the two-particle density have also been proposed [46, 47].

5. Conclusion

An imaginary-time evolution method has been employed to obtain nonrelativistic ground-state electronic densities and energies for all the noble gas atoms through the solution of a single diffusion-type equation in appropriately scaled cylindrical coordinates. The radial densities and associated energy terms are strictly spherically symmetric and reveal all the expected features. The calculated properties are in close agreement with those from the literature. The algorithm can be readily applied for studying the dynamics of similar systems in real time subjected to external fields in terms of the electron density in three-dimensional space. This would entail solving a single equation under the influence of a single effective potential compared to solving a number of equations and thus should enable one to tackle more complex systems with a relatively large number of electrons. Furthermore, since the calculations are performed in a realistic and flexible set of scaled cylindrical coordinates, the three-dimensional portrayal of the dynamics can be visualized in real time throughout the evolution process, thereby facilitating a detailed probing of electronic motions necessary for understanding attosecond phenomena.

Acknowledgments

AP takes pleasure in thanking Dr Howard Cohl for helpful correspondence concerning the calculation of the interelectronic Coulomb repulsion potential in scaled cylindrical coordinates. He also thanks the UGC, New Delhi, for financial support.

References

- [1] Parr R G and Yang W 1989 *Density Functional Theory of Atoms and Molecules* (New York: Oxford University Press)
- [2] Bamzai A S and Deb B M 1981 *Rev. Mod. Phys.* **53** 95, 593
- [3] Deb B M and Ghosh S K 1987 *The Single Particle Density in Physics and Chemistry* ed N H March and B M Deb (London: Academic) p 219
- [4] Thomas L H 1927 *Proc. Camb. Phil. Soc.* **23** 542
- [5] Fermi E 1928 *Z. Phys.* **48** 73
- [6] Deb B M and Chattaraj P K 1989 *Phys. Rev. A* **39** 1696
- [7] Ullrich C A, Grossman U J and Gross E K U 1995 *Phys. Rev. Lett.* **74** 872
- [8] Tong X M and Chu S I 2001 *Phys. Rev. A* **63** 023411
- [9] Telnov D and Chu S I 1998 *Phys. Rev. A* **58** 4749
- [10] Roy A K, Dey B K and Deb B M 1999 *Chem. Phys. Lett.* **308** 523
- [11] Dey B K and Deb B M 1999 *J. Chem. Phys.* **110** 6229
- [12] Roy A K and Chu S I 2002 *J. Phys. B: At. Mol. Opt. Phys.* **35** 2075
- [13] Dey B K and Deb B M 1995 *Int. J. Quantum Chem.* **56** 707
- [14] Dey B K and Deb B M 1998 *Int. J. Quantum Chem.* **70** 441
- [15] Chattaraj P K, Sengupta S and Poddar A 1998 *Int. J. Quantum Chem.* **69** 279
- [16] Wadehra A and Deb B M 2006 *Eur. Phys. J. D* **39** 141
- [17] Roy A K and Chu S I 2002 *Phys. Rev. A* **65** 043402
- [18] Shan B and Chang Z 2001 *Phys. Rev. A* **65** 011804
- [19] Gavrilla M 2002 *J. Phys. B: At. Mol. Opt. Phys.* **35** R147
- [20] Valentin C, Kazamias S, Doulliet D, Grillon G, Lefrou Th, Auge A, Lewenstein M, Wyart J F, Sebban S and Balcou Ph 2004 *J. Phys. B: At. Mol. Opt. Phys.* **37** 2661
- [21] Scrinzi A, Ivanov M Y, Kienberger R and Villeneuve D M 2006 *J. Phys. B: At. Mol. Opt. Phys.* **39** R1
- [22] Deb B M and Ghosh S K 1983 *Int. J. Quantum Chem.* **23** 1
- [23] Gross E P 1961 *Nuovo Cimento* **20** 454
- [24] Pitaevskii L P 1961 *Sov. Phys.—JETP* **13** 451
- [25] Hammond B L, Lester W A Jr and Reynolds P J 1994 *Monte Carlo Methods in Ab Initio Quantum Chemistry* (Singapore: World Scientific)
- [26] Roy A K, Gupta N and Deb B M 2002 *Phys. Rev. A* **65** 012109
- [27] Roy A K, Wadehra A and Deb B M 2003 *Int. J. Quantum Chem.* **91** 597
- [28] Roy A K, Thakkar A J and Deb B M 2005 *J. Phys. A: Math. Gen.* **38** 2189
- [29] Gupta N and Deb B M 2006 *Chem. Phys.* **327** 351
- [30] Ghosh S K and Deb B M 1994 *J. Phys. B: At. Mol. Opt. Phys.* **27** 381
- [31] Singh R and Deb B M 1996 *J. Chem. Phys.* **104** 5892
- [32] Cohl H S and Tohline J E 1999 *Astrophys. J.* **527** 86
- [33] Morse P and Feshbach H 1953 *Methods of Theoretical Physics* (New York: McGraw-Hill)
- [34] Abramowitz M and Stegun I A 1965 *Handbook of Mathematical Functions with Formulas, Graphs and Mathematical Tables* (New York: Dover)
- [35] Kono H, Kita A, Ohtsuki Y and Fujimura Y 1997 *J. Comput. Phys.* **130** 148
- [36] Kono H, Kawata I and Fujimura Y 2000 *RIKEN Rev.* **29** 60
- [37] Mitchell A R 1976 *Computational Methods in Partial Differential Equations* (London: Wiley) chapters 2 and 3
- [38] Press W H, Teukolsky S A, Vetterling W T and Flannery B P 1988 *Numerical Recipes* (Cambridge: Cambridge University Press)
- [39] Adams J, Swartztrauber P and Sweet R <http://www.scd.ucar.edu/css/software/fishpack/>
- [40] Vikas 2004 Time-independent and time-dependent studies of quantum mechanical systems *PhD Thesis* Punjab University, Chandigarh, India (corrigendum)
Vikas and Deb B M 2004 *Int. J. Quantum Chem.* **97** 701 (see footnote)
- [41] Singh R and Deb B M 1999 *Phys. Rep.* **311** 47

-
- [42] Chattaraj P K and Deb B M 1984 *J. Sci. Ind. Res.* **43** 238
 - [43] March N H 1986 *Phys. Lett.* **113A** 476
 - [44] Chan G K-L and Handy N C 2000 *J. Chem. Phys.* **112** 5639
 - [45] Chan G K-L, Cohen A J and Handy N C 2001 *J. Chem. Phys.* **114** 631
 - [46] Furche F 2004 *Phys. Rev. A* **70** 022514
 - [47] Ayers P W 2005 *J. Math. Phys.* **46** 062107